# Efficient multi-wavelength lasers made of Nd:GdLuAG crystal

**Yongguang Zhao (赵永光)[1], Zhengping Wang (王正平)[2,*], Haohai Yu (于浩海)[2], Xiaodong Xu (徐晓东)[3], Jun Xu (徐 军)[3], and Xinguang Xu (许心光)[2]**

[1]*Key Laboratory of Advanced Laser Materials and Devices, School of Physics and Electronic Engineering, Jiangsu Normal University, Xuzhou 221116, China*

[2]*State Key Laboratory of Crystal Materials and Institute of Crystal Materials, Shandong University, Jinan 250100, China*

[3]*Key Laboratory of Transparent and Opto-Functional Inorganic Materials, Shanghai Institute of Ceramics, Chinese Academy of Sciences, Shanghai 201800, China*

**Corresponding author: zpwang@sdu.edu.cn*

Received October 4, 2014; accepted November 14, 2014; posted February 6, 2015

Owing to the small differences between the cross-sections of the four emission peaks around 1.3 μm, an efficient four-wavelength synchronous launched laser is demonstrated using a Nd:GdLuAG crystal. The laser has no special resonator design. The maximum output power is 4.28 W, which corresponds to a conversion efficiency of 45.6%. For the *Q*-switching, the laser operated in dual-wavelength mode, and the single pulse energy is maintained at ∼80 μJ. By calculating the population inversion density, multi-wavelength emission characteristics in both continuous wave and *Q*-switching lasers are discussed.

*OCIS codes: 140.3380, 140.3540, 300.2530.*
*doi: 10.3788/COL201513.021404.*

Gain materials are crucial for fostering the development and applications of lasers. In gain materials, the emission by active ions is determined mainly by their electronic structure, and is modulated by the crystal field of the host material[1]. Garnet crystals have been identified as the most prominent hosts, since they have excellent chemical and physical properties. As a representative, Nd:YAG has become a commercial success. Nowadays, more research on these materials is focused on the multiple-wavelengths laser emission, due to its desirability for a wide range of applications, including precision spectral analysis, medical instrumentation, and optical clock synchronization. Host cation doping is an effective method for increasing the emissive center and adjusting the stimulated emission cross-section of the active ions, such as Nd-doped $GdYVO_4$[2], $LuYSiO_4$[3], $YGd_2Sc_2Al_2GaO_{12}$[4], and so on. A $Nd_{0.03}$:$Lu_{2.871}Gd_{0.099}Al_5O_{12}$ crystal was first grown in 2011 as a novel host cation doping laser material, and its laser properties at 1.06 and ∼0.95 μm were simply demonstrated in 2011[5] and 2013[6], respectively. To our knowledge, these are all of the results about this laser crystal. Its emission property of an $^4F_{3/2} \rightarrow {}^4I_{13/2}$ transition has never been reported. Compared to the fluorescence spectrum of the well-known Nd:YAG crystal, the intensity differences among the four emission peaks around 1.3 μm in $Nd_{0.03}$:$Lu_{2.871}Gd_{0.099}Al_5O_{12}$ are even smaller, which is beneficial to realizing multi-wavelength lasing. More importantly, by a random replacement of Lu ions with Gd ions, a disordered structure can be created, which should be favorable for producing large-pulse energy in a *Q*-switching laser and a short pulse duration in a mode-locking laser.

In this Letter, by using a commercial laser diode as pump source, a four-wavelength laser around 1.3 μm was demonstrated with a Nd:LuGdAG crystal in a simple two-mirror cavity. To our knowledge, this is the first time that a research team has obtained the four-wavelength laser emission by using these double-cations doping laser materials. For the *Q*-switching laser operation, a dual-wavelength laser with the largest pulse energy, ∼80 μJ, was demonstrated. These simultaneous multi-wavelength lasers are the best choice to generate the ultrahigh repetition rate pulses by optical beating[7,8] and the coherent terahertz radiation by difference frequency generation[9,10].

A Nd:GdLuAG ($Nd_{0.03}Lu_{2.871}Gd_{0.099}Al_5O_{12}$) crystal was grown using the Czochralski process. It has a cubic structure with the space group of $O_h^{10}$-Ia3d, which means that the optical properties are independent of the crystal orientation. The crystal is cut along its ⟨111⟩ direction with the dimension of 3 mm × 3 mm × 6 mm. Its two 3 mm × 3 mm end faces are polished and uncoated. An Edinburgh FS920 High Sensitive Fluorescence Spectrometer is used to measure the fluorescence spectra. The pump source is a xenon lamp with an emission wavelength of 200–900 nm, and the detector is a 800–1700 nm InGaAs stable-state detector with a resolution of <0.09 nm (with a 1200 g/mm grating). The emission light data of the crystal is measured at room temperature with the step length of 0.1 nm. Figure 1 shows the fluorescence spectrum of the Nd:GdLuAG crystal; the inset is the fine spectrum of $Nd^{3+}$ in the $^4F_{3/2} \rightarrow {}^4I_{13/2}$ transition. Four emission peaks at 1321.1, 1333.4, 1338.5, and 1353 nm are found in the $^4F_{3/2} \rightarrow {}^4I_{13/2}$ transition, corresponding to the fine transition of $R_2 \rightarrow X_2$, $R_1 \rightarrow X_1$, $R_2 \rightarrow X_3$, and $R_1 \rightarrow X_4$,

 

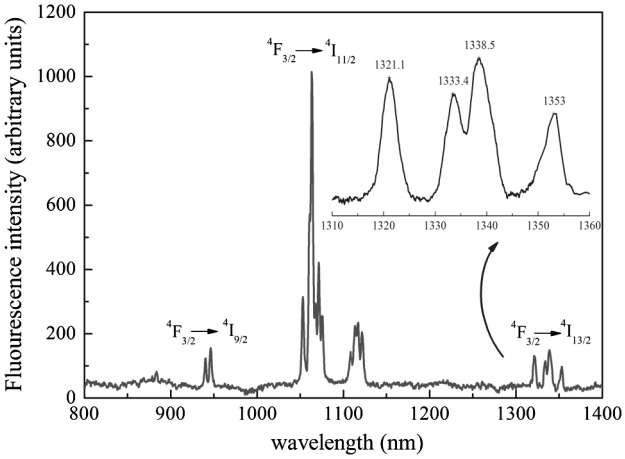


Fig. 1. Fluorescence spectrum of the Nd:GdLuAG crystal at room temperature. Inset: Fine spectrum of the $^4F_{3/2} \rightarrow {}^4I_{13/2}$ transition.

respectively. With the fluorescence lifetime of $\tau_r = 262$ μs measured[5], the stimulated emission cross-sections can be calculated by Fuchtbauer–Ladenbrug method[11,12]:

$$\sigma_e(\lambda) = \frac{\lambda^4 I(\lambda)}{8\pi c n^2 \tau_r \int I(\lambda) \mathrm{d}\lambda}, \quad (1)$$

where $I(\lambda)$ is the fluorescence intensity at the wavelength $\lambda$, and $n$ is the refractive index. The calculated results of 1321.1, 1333.4, 1338.5, and 1353 nm were $1.7 \times 10^{-20}$, $1.5 \times 10^{-20}$, $2.0 \times 10^{-20}$, and $1.4 \times 10^{-20}$ cm$^2$, respectively. The comparable values of $\sigma$ make it possible to obtain simultaneous multi-wavelength oscillation around 1.3 μm. Moreover, the values are smaller than that of the Nd:YAG crystal ($8.7 \times 10^{-20}$ cm$^2$ for 1318.8 nm, and $9.2 \times 10^{-20}$ cm$^2$ for 1338.2 nm[13]). Combined with the relative longer fluorescence lifetime, Nd:GdLuAG has a larger energy storage capacity and is more capable of producing large pulse energy and high-peak power lasers.

Figure 2 shows the experimental setup. The pump source was a fiber-coupled laser diode with a central wavelength at approximately 808 nm. The numerical aperture of the fiber bundle was 0.22, and the output of the source was focused onto the laser crystal with a spot radius of 0.1 mm. M1 was the input mirror with a curvature radius of 250 mm. M1 was high-transmission (HT) coated at 808 nm and 1.06 μm on the flat face, and HT-coated at 808 nm and 1.06 μm and high-reflection coated at 1310–1360 nm on the concave face. The output couplers of M2 were flat mirrors with different transmission lengths ranging from 1310 to 1360 nm ($T \approx 1\%, 3.4\%, 6.3\%$, and $11.2\%$; the values at specific wavelengths can be seen in Fig. 2). The Nd:GdLuAG crystal was polished and uncoated. To remove the generated heat under high pump powers, the laser crystal was wrapped in indium foil and mounted on a water-cooled copper block, and the saturable absorber was held in a copper block without cooling water. The $V^{3+}$:YAG absorber, with the dimensions of 3 mm × 3 mm × 2.8 mm and an initial transmission of 95% at 1.34 μm, was placed next to M2, to realize the $Q$-switching laser operation. The generated continuous wave (CW) and pulsed average output powers were measured using an energy/power meter (Molectron, EPM 2000). The temporal behaviors of the $Q$-switched laser were recorded using a DPO7104 digital oscilloscope (1 GHz bandwidth and 10 Gs/s sampling rate, Tektronix) and a photo-detector (New focus, model 1611). The spectral information was monitored by a commercial optical spectrum analyzer (Yokogawa, AQ6370 C) with a resolution of 0.05 nm.

Without the $V^{3+}$:YAG, the laser was in the CW regime. Figure 3(a) shows the output power as a function of the absorbed pump power. The maximum output power of 4.28 W was obtained when $T = 3.4\%$, corresponding to a conversion efficiency of 45.6%. We assume the mode volume efficiency between the pump and the laser modes is equal to the value of $(\omega_{l,i}^2 + \omega_p^2)l$[14], where $w_{l,i}$ and $w_p$ are the beam radii for the laser and the pump modes at the

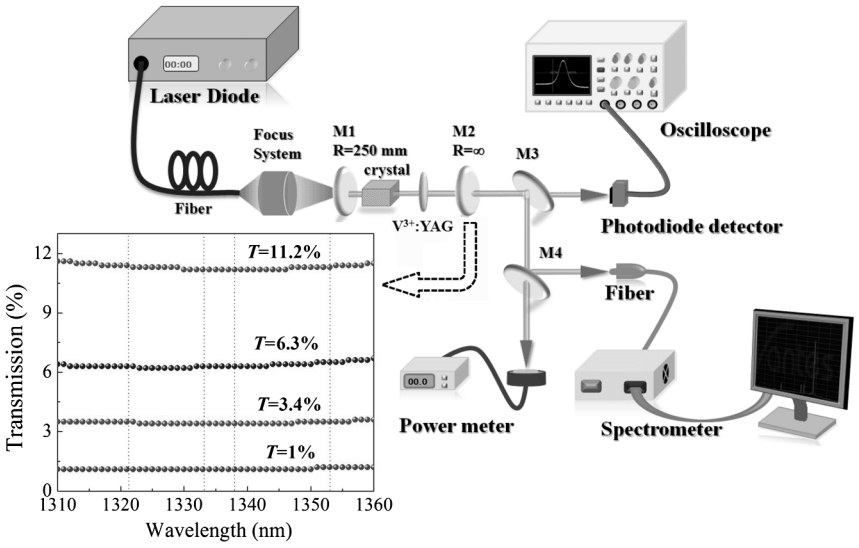


Fig. 2. Schematic diagram of the experimental setup, and the transmission of the different output couplers used in this experiment.

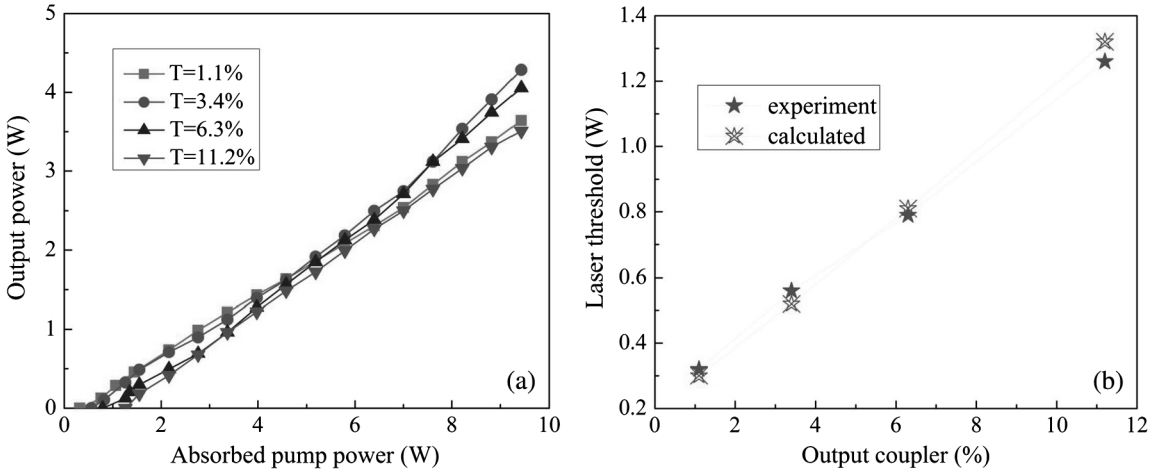


Fig. 3. (a) Output power as a function of the absorbed pump power. (b) The calculated initial laser thresholds at different wavelengths, and the experimental results at 1338 nm.

waist in the active medium, respectively, and $l$ is the crystal length. According to the gain and total cavity round-trip loss, the threshold for each transition in a four-level laser can be expressed as[15]

$$P_{th,i} = \frac{\ln(\frac{1}{R_i}) + L_i}{2\eta_i} \frac{h\nu_p}{\sigma_i \tau_i} (\omega_{l,i}^2 + \omega_p^2), \qquad i = 1, 2, 3, 4, \quad (2)$$

where $i = 1$, 2, 3, and 4 represent the modes at 1338.4, 1320.5, 1333.4, and 1353 nm, respectively; $R$ is the reflectivity of M2 and is shown in Fig. 2; $L$ is the round-trip cavity loss; $\eta$ is the quantum efficiency; $\sigma$ is the emission cross-section; $\tau$ is the fluorescence lifetime at the upper level. Comparing the calculated results of the four transitions, the mode at 1338 nm has the minimum threshold and oscillated first. As shown in Fig. 3(b), the calculated values at 1338 nm with different output couplers are joined well with our experiment, which indicates that the laser cavity has been optimized well. Once the first oscillated mode was obtained, the laser thresholds of the other modes could not be calculated by Eq. (2). The main reason was that mode at 1338.4 nm fixes the population inversion at a level which is below that required to obtain lasing from the other modes, which can oscillate only at a much higher pump power, due to the nonhomogeneity of the population inversion in the gain medium. When $T = 3.4\%$, the experimental thresholds at 1320.5, 1333, 1353 nm are 1.02, 3.62, and 7.18 W, respectively.

With a high-resolution spectrum analyzer (Yokogawa, AQ6370 C), the laser spectra were recorded and shown in Fig. 4. By increasing the pump power, we can obtain single-, dual-, tri-, and four-wavelengths laser outputs, respectively. The different frequency interactions among these wavelengths may be used to generate radiation at 0.84, 2.2, 2.42, 3.04, 3.26, and 5.46 THz.

By inserting the $V^{3+}$:YAG as the saturable absorber, a 1.3 μm, passive $Q$-switched laser was realized. The average output power at different output couplers versus the absorbed pump power is shown in Fig. 5(a). The maximum output power of 1.7 W was obtained when $T = 6.3\%$. The relatively large threshold of 2.21 W was due to the large threshold population inversion density caused by the small stimulated emission cross-section and the uncoated insert loss[16]. Fortunately, the large thermal conductivity and the excellent crystal quality allowed it to still run under high-pump power. With a DPO7104 digital oscilloscope, the laser pulse was recorded. Figure 5(b) shows the pulse width versus the width of the absorbed pump power. The shortest pulse width, 21.8 ns, was obtained at the highest pump power, when $T = 3.4\%$, and the profile is shown in the inset of Fig. 5(b). Using the average output power and the pulse repetition frequency (PRF), the single pulse energy was calculated. Its variation with the absorbed pump power is shown in Fig. 5(c). The pulse energy was stable, and the variation was less than 10%, unlike its tendency to rise, as seen in Refs. [17,18]. Instead, it is similar to the case found by Chen and Lan[19,20]. In this

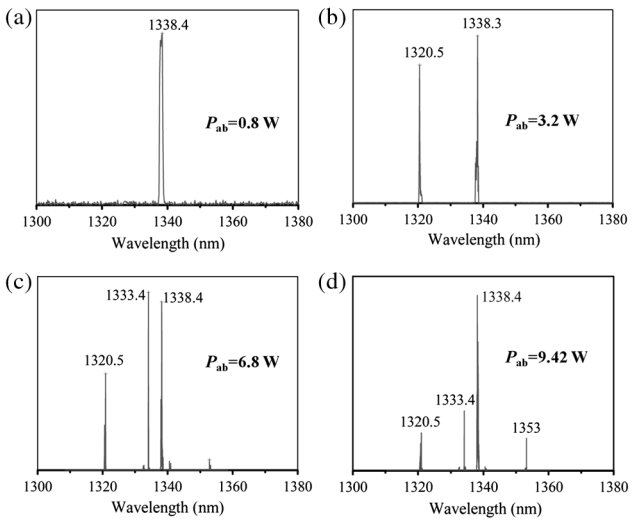


Fig. 4. Laser spectra at different absorbed pump powers when $T = 3.4\%$: (a) $P_{ab} = 0.8$ W. (b) $P_{ab} = 3.2$ W. (c) $P_{ab} = 6.8$ W. (d) $P_{ab} = 9.42$ W.

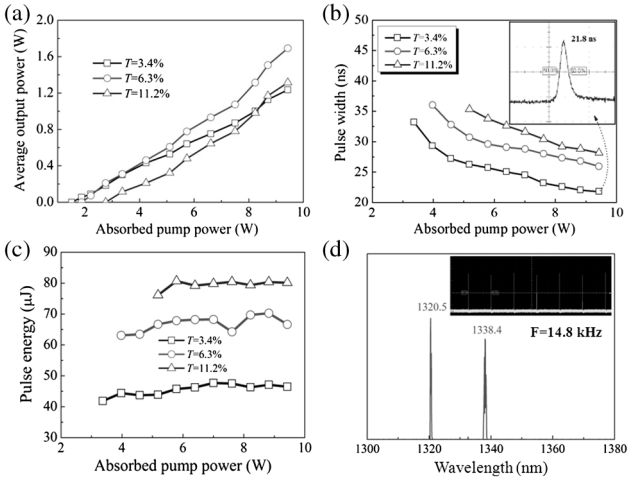


Fig. 5. Characterization of the passive $Q$-switching laser. (a) Average output power versus the absorbed pump power. (b) Pulse width as a function of the absorbed pump power; inset: pulse profile of 21.8 ns. (c) Pulse energy versus the absorbed pump power. (d) Laser spectrum of the passive $Q$-switched dual-wavelength laser at the absorbed pump power of 9.42 W; inset: the pulse trains at 14.8 kHz.

experiment, the largest pulse energy was obtained when $T = 11.2\%$, and was maintained at ~80 μJ. The results are improved over those obtained in the case of the Nd:YAG crystal ($37 \pm 7$ ns, 25 μJ)[18] and the ceramic (~140 ns, 51 μJ with $T_0 = 90\%$)[21]. In these cases, the results were mainly caused by the smaller stimulated emission cross-section, and the longer upper level lifetime. The uniformity of the pulse trains, as shown in Fig. 5(d), indicated the stability of the passive $Q$-switching lasers with this novel laser gain. With a mirror that has different reflectivity at 1320.5 and 1338.4 nm, no time jitter or amplitude fluctuations were found in the pulse trains after the output laser had passed by. During combing with the pulse profile, no optical beating between the dual wavelengths was observed, and no satellite pulse was present before or after the pulse. We believe the pulses of the dual wavelengths are time-overlapped.

As recorded by the spectrum analyzer, the laser first oscillated in a single-wavelength mode, and the second wavelength turned out as the pump power increased. The recorded dual wavelength when $T = 3.4\%$ at 1338.4 and 1320.5 nm is shown in Fig. 5(d). No third wavelength was observed, which was not the situation in the CW laser operation. As discussed in Refs. [22,23], the $i$th mode initial population inversion density $n_{ii}$ of the pulsed laser of the passive $Q$-switching laser can be written as

$$n_{ii} = \frac{\ln\left(\frac{1}{1-T_i}\right) + \ln\left(\frac{1}{T_0^2}\right) + L_i}{2\sigma_i l}. \tag{3}$$

The initial population inversion density of the different wavelengths versus the output coupler $T$ and initial transmissions $T_0$ is shown in Fig. 6 (left). The value of $n_{ii}$ increased as the value of $T_0$ decreased, or as the output coupler increased. $n_{ii=1338.4}$ is always smaller than the other three modes, which means that the laser oscillates more easily at 1338.4 nm. Once the laser is generated, the transmission of V:YAG becomes saturated and is "bleached" by the laser at 1338.4 nm. Then the other mode will oscillate if the residual population inversion density $n_{ri}$ has reached its threshold. $n_{ri}$ can be expressed by

$$n_{ri} = \frac{\ln\left(\frac{1}{1-T_i}\right) + \ln\left(\frac{1}{T_s^2}\right) + L_i}{2\sigma_i l}, \tag{4}$$

where $T_s$ is the saturated transmission of V:YAG. For $T_0 = 0.95$ in the present experiment, the total population inversion density of $n_{ii=1338.4}$ and $n_{ri}$ ($i = 1320.5, 1334.4,$ or 1353 nm) is calculated by Eq. (4) and shown in Fig. 6 (right). At each output coupler, $n_{ii=1338.4} + n_{ri=1320.5}$ is the minimum, which indicates that the threshold of 1320.5 nm is smaller than that of 1333.4 and 1353 nm. In this experiment, the laser oscillated at 1320.5 nm as the second mode

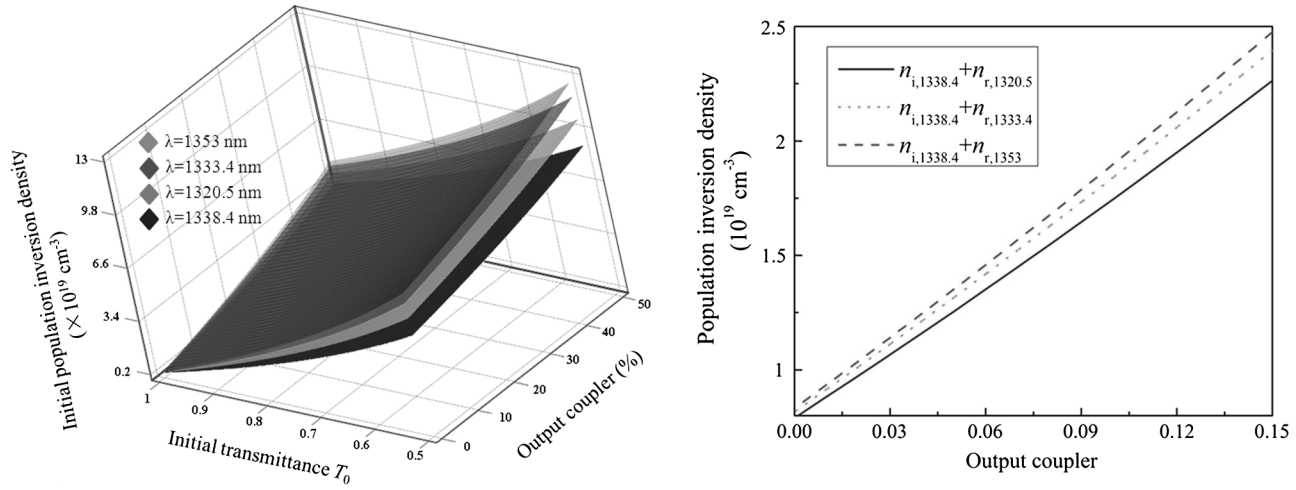


Fig. 6. Initial population inversion density versus the initial transmittance of the absorber and the output coupler (left). Total population inversion density at the different couplers (right).

at different output couplers, but the third wavelength was not observed as being limited by the absorbed pump power. According to our calculations, the third and even the forth wavelength may appear when the output coupler $T$ is decreased, and/or when the initial transmissions $T_0$ are increased.

In conclusion, we research the 1.3 μm spontaneous and stimulated emission characteristics of a novel Nd:GdLuAG crystal. The stimulated emission cross-sections are calculated according to the measured fluorescence spectrum. Their values are $1.7 \times 10^{-20}$ , $1.5 \times 10^{-20}$ , $2.0 \times 10^{-20}$ , and $1.4 \times 10^{-20}$ $\mathrm{cm}^2$ for the four emission peaks at 1321.1, 1333.4, 1338.4, and 1353 nm, respectively. CW and passive $Q$-switched lasers at 1.3 μm with this novel crystal are also demonstrated. In the CW operation, the laser operates in single-, dual-, tri-, and four-wavelengths, in order with the increasing pump power. The maximum output power obtained is 4.28 W when $T = 3.4\%$, which corresponds to a conversion efficiency of 45.6%. By using a $V^{3+}$:YAG as a saturable absorber, a passive $Q$-switched dual-wavelength laser is realized at 1320.5 and 1338.5 nm. Then, the select wavelength characteristics are examined by calculating the threshold and population inversion density in the CW and $Q$-switching lasers, respectively. In the pulsed laser operation, the single pulse energy is stable and basically insensitive to the pump power, and the largest pulse energy is maintained at ∼80 μJ when $T = 11.2\%$. This dual-wavelength laser, with its large, stable pulse energy and time synchronization, may be used in various fields, including material processing, nonlinear frequency conversion, high-energy physics, and differential interferometry synthetic aperture radar.

This work was supported by the National Natural Science Foundation of China (No. 61178060), the Program for New Century Excellent Talents in University (No. NCET-10-0552), the Independent Innovation Foundation of Shandong University (No. 2012TS215), and the Natural Science Foundation for Distinguished Young Scholars of Shandong Province (No. 2012JQ18).

## References

1. M. J. Weber, J. D. Myers, and D. H. Blackburn, J. Appl. Phys. **52**, 2944 (1981).
2. Y. Zhao, H. Yu, Z. Wang, H. Zhang, X. Xu, and J. Wang, J. Opt. Soc. Am. B **30**, 1241 (2013).
3. Y. Zhao, S. Zhuang, X. Xu, J. Xu, H. Yu, Z. Wang, and X. Xu, Opt. Express **22**, 2228 (2014).
4. G. Alombert-Goget, A. Brenier, Y. Guyot, A. LabruyŁre, B. Faure, and V. Couderc, Opt. Express **22**, 10792 (2014).
5. J. Di, X. Xu, D. Li, D. Zhou, F. Wu, Z. Zhao, J. Xu, and D. Tang, Laser Phys. **21**, 1742 (2011).
6. S. Zhuang, S. Han, Z. Wang, D. Hu, X. Xu, H. Yu, J. Xu, and X. Xu, IEEE Photon. Technol. Lett. **25**, 355 (2013).
7. M. D. Pelusi, H. F. Liu, D. Novak, and Y. Ogawa, Appl. Phys. Lett. **71**, 449 (1997).
8. G. Xie, D. Tang, H. Luo, H. Zhang, H. Yu, J. Wang, X. Tao, M. Jiang, and L. Qian, Opt. Lett. **33**, 1872 (2008).
9. K. Miyamoto, H. Minamide, M. Fujiwara, H. Hashimoto, and H. Ito, Opt. Lett. **33**, 252 (2008).
10. D. Creeden, J. C. McCarthy, P. A. Ketteridge, P. G. Schunemann, T. Southward, J. J. Komiak, and E. P. Chicklis, Opt. Express **15**, 6478 (2007).
11. B. F. Aull and H. P. Jenssen, IEEE J. Quantum Electron. **18**, 925 (1982).
12. G. Turri, H. P. Jenssen, F. Cornacchia, M. Tonelli, and M. Bassi, J. Opt. Soc. Am. B **26**, 2084 (2009).
13. S. Singh, R. G. Smith, L. G. Van, and V. Vitert, Phys. Rev. B **10**, 2566 (1974).
14. G. Shayeganrad and L. Mashhadi, Appl. Phys. B **111**, 189 (2013).
15. T. Y. Fan and R. L. Byer, IEEE J. Quantum Electron. **24**, 895 (1988).
16. X. Y. Zhang, S. Z. Zhao, and Q. P. Wang, J. Opt. Soc. Am. B **17**, 1166 (2000).
17. T. T. Kajava and A. L. Gaeta, Opt. Lett. **21**, 1244 (1996).
18. A. V. Podlipensky, K. V. Yumashev, N. V. Kuleshov, H. M. Kretschmann, and G. Huber, Appl. Phys. B **76**, 245 (2003).
19. Y. F. Chen and Y. P. Lan, Appl. Phys. B **79**, 29 (2004).
20. Y. F. Chen and Y. P. Lan, Appl. Phys. B **74**, 415 (2002).
21. T. Omatsu, A. Minassian, and M. J. Damzen, Opt. Comm. **282**, 4784 (2009).
22. J. J. Degnan, IEEE J. Quantum Electron. **31**, 1890 (1995).
23. X. Zhang, S. Zhao, Q. Wang, Q. Zhang, L. Sun, and S. Zhang, IEEE J. Quantum Electron. **33**, 2286 (1997).